Polarized infrared emissivity of one-dimensional Gaussian sea surfaces with surface reflections

Hongkun Li,* Nicolas Pinel, and Christophe Bourlier

Université de Nantes–IREENA Laboratory, Ecole Polytechnique de L'Université de Nantes, Rue Christian Pauc, La Chantrerie, BP 50609, 44306 Nantes Cedex 3, France

*Corresponding author: hongkun.li@etu.univ-nantes.fr

Received 20 December 2010; revised 13 May 2011; accepted 16 June 2011; posted 5 July 2011 (Doc. ID 139882); published 4 August 2011

Surface reflection is an important phenomenon that must be taken into account when studying sea surface infrared emissivity, especially at large observation angles. This paper models analytically the polarized infrared emissivity of one-dimensional sea surfaces with shadowing effect and one surface reflection, by assuming a Gaussian surface slope distribution. A Monte Carlo ray-tracing method is employed as a reference. It is shown that the present model agrees well with the reference method. The emissivity calculated by the present model is then compared with measurements. The comparisons show that agreements are greatly improved by taking one surface reflection into account. The Monte Carlo ray-tracing results of sea surface infrared emissivity with two and three reflections are also determined. Their contributions are shown to be negligible. © 2011 Optical Society of America

OCIS codes: 290.5880, 000.5490, 010.4450, 260.3060, 280.0280.

1. Introduction

Infrared emissivity of oceanic surfaces in atmospheric transmission windows is an important parameter in environment remote sensing. Direct infrared emissivity (named zero-order, as no surface reflection is considered) of sea surfaces has already been studied thoroughly. The shadowing effect is essential when studying the direct emissivity of a rough surface and, in particular, at large observation angles. The model of Masuda *et al.* [1] introduced a shadowing term to evaluate the shadowing effect, whereas Bourlier [2] employed a shadowing function. Fauqueux *et al.* [3] developed a multiresolution model of sea infrared emissivity, in which the shadowing term of Masuda *et al.* was used.

In practice, it is necessary to obtain the sea surface emissivity with an accuracy of 5×10^{-3} [4]. However, this accuracy is not achieved by direct emissivity models. Compared with experimental data obtained by Smith *et al.* [5] and Niclòs *et al.* [6], the direct emissivity model of Masuda *et al.* [1] shows a difference of about $2–3 \times 10^{-2}$ at large observation angles. As a result, it is necessary to take the emissivity with surface reflections into account.

Several authors tried to include surface reflections in their emissivity models. The main difficulty lies in the derivation of the probability of observing surface reflections, which is called the nth-order illumination function, where n denotes the number of surface reflections. Instead of using a high-order illumination function, Watts *et al.* [7] and Wu and Smith [4] both defined empirically the probability of observing surface reflections by defining an ambiguous cutoff angle. As little information is available to help define the cutoff angle, the resulting emissivity greatly changes with the cutoff angle value, which leads to a large uncertainty. Masuda [8] built a weighting function so that he did not have to define an exact cutoff angle. However, the resulting emissivity with one surface reflection does not agree with the result computed from the Monte Carlo ray-tracing method (see Subsection 4.C for discussion). Henderson *et al.* [9] developed a Monte Carlo ray-tracing method to evaluate sea surface emissivity with surface reflections. The Monte Carlo ray-tracing model gives

0003-6935/11/234611-11$15.00/0

reliable results for infrared wavelengths, but the disadvantage is that the computation time is much longer [10] than that of an analytical model. Bourlier [11] developed a statistical nth-order illumination function to calculate the sea infrared emissivity with surface reflections. It is shown that Bourlier's first-order illumination function underestimates the surface reflection effect. In consequence, the first-order emissivity is also underestimated. Li *et al.* [10] developed a first-order illumination function whose result agrees very well with that of a Monte Carlo ray-tracing method. It can be promising to derive the first-order emissivity by adopting this illumination function.

The above emissivity models do not take polarization into account, except for that of Henderson *et al.* [9]. It is reported that infrared emission of sea surfaces is partially polarized at large observation angles [12,13]. Shaw and Marston [13] determined the degree of polarization (DOP) of the sea surface infrared emissivity from the direct emissivity model of Masuda *et al.* [1]. However, surface reflections are not taken into account.

This paper develops an analytical model that determines the infrared emissivity with one reflection of a one-dimensional (1D) sea surface, by adopting the statistical first-order illumination function of Li *et al.* [10] and the emissivity model of Bourlier [11]. Polarization is also taken into account. The geometric optics approximation (GO), which describes the rough surface as a series of continuous smooth facets, is assumed to be valid, which means that specular reflections are considered. All the angles in this paper are oriented, with clockwise being the positive direction.

This paper is organized as follows: in Section 2, emissivity without surface reflection is briefly recalled. In Section 3, emissivity with one surface reflection is derived. Polarization is taken into account, and the DOP is derived. In Section 4, numerical results of the infrared emissivity are simulated and compared with the results of a Monte Carlo ray-tracing method and then with measurements. Section 5 gives concluding remarks.

2. Emissivity without Surface Reflections

Zero-order (without surface reflections) infrared emissivity of a rough surface has been well studied [1–3]. In this section, the statistical model of Bourlier [2] is adopted and summarized, and it is extended later to higher orders (with surface reflections).

The GO is valid if [14]

$$2\pi\rho_c \cos^3\chi_0 \gg \lambda, \tag{1}$$

where λ is the studied wavelength and ρ_c is the surface local radius of curvature. χ_0 is the local incidence angle, corresponding to the angle between the normal to the facet and the observation direction. This paper deals with the infrared domain, which means that λ is of the order of $10\,\mu$m. The surface local radius of curvature ρ_c of the capillary waves of the sea surface is of the order of 1 cm. In this case, Eq. (1) is valid for $\cos\chi_0 \gg 0.025$, which corresponds to a local incidence angle close to 90° ($\cos 88.5° \approx 0.025$). As a result, the GO is assumed to be valid throughout the paper.

In this paper, a 1D rough surface is considered. The geometry of the zero-order emissivity is shown in Fig. 1. A coordinate system xz is defined, with $\hat{\mathbf{x}}$ being the horizontal direction toward the sensor and $\hat{\mathbf{z}}$ being the zenith direction.

An arbitrary point M_0 of the rough surface, with height ζ_0 and slope γ_0, is considered. The ray $M_0(\theta)$ is the emission ray, with θ being the observation angle. The vector $\hat{\mathbf{n}}_0 = (-\gamma_0, 1)/(1+\gamma_0^2)^{1/2}$ is the unitary normal vector of the facet at point M_0. The unitary vector of the emission ray $M_0(\theta)$ is denoted as $\hat{\mathbf{m}}_0 = (\sin\theta, \cos\theta)$. Thus, the local incidence angle χ_0 is given by

$$\cos\chi_0 = \hat{\mathbf{n}}_0 \cdot \hat{\mathbf{m}}_0 = \frac{\cos\theta - \gamma_0 \sin\theta}{(1+\gamma_0^2)^{1/2}}. \tag{2}$$

The zero-order infrared emissivity of a 1D surface is given by [2]

$$\varepsilon_{0,V,H} = \langle [1 - |r_{V,H}(\chi_0)|^2] g_0 S_0(\mu, \gamma_0, \zeta_0) \rangle_0, \tag{3}$$

where $\langle \cdots \rangle_0$ stands for the zero-order statistical average:

$$\langle \cdots \rangle_0 = \int_{-\infty}^{+\infty} \int_{-\infty}^{+\infty} \cdots p(\zeta_0, \gamma_0) \mathrm{d}\zeta_0 \mathrm{d}\gamma_0, \tag{4}$$

where $p(\zeta, \gamma)$ is the joint probability density function (PDF) of the heights and the slopes of the surface.

The term $[1 - |r_{V,H}(\chi_0)|^2]$ is the zero-order local emissivity of the facet at point M_0, where $r_{V,H}$ is the Fresnel reflection coefficient. The subscripts V and H stand for V polarization (the electric vector is parallel to the plane of incidence) and H polarization (the electric vector is orthogonal to the plane of incidence), respectively. The Fresnel reflection coefficients are given by

$$r_V(\chi) = \frac{n\cos\chi - \cos\chi'}{n\cos\chi + \cos\chi'}, \quad r_H(\chi) = \frac{\cos\chi - n\cos\chi'}{\cos\chi + n\cos\chi'}, \tag{5}$$

where n is the sea refraction index. χ is the local incidence angle, whereas χ' is the local refraction angle given by Snell's law: $\sin(\chi') = \sin(\chi)/n$.

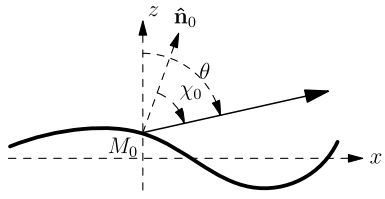

Fig. 1. Geometry of zero-order emissivity (without surface reflection).

The term g_0 in Eq. (3) results from projecting the area of the facet onto the orthogonal direction of the observation direction. It is given by

$$g_0 = 1 - \gamma_0 \tan\theta. \tag{6}$$

$S_0(\mu, \gamma_0, \zeta_0)$ is the zero-order illumination function, which gives the probability that point M_0 is viewed by the sensor. In this paper, the illumination function of Smith [15] is adopted. It is given by

$$S_0(\mu, \gamma_0, \zeta_0) = \Upsilon(\mu - \gamma_0) F(\zeta_0)^{\Lambda(\mu)}, \tag{7}$$

where $\mu = \cot\theta$ is the slope of the emission ray. $F(\zeta)$ is the surface height ζ cumulative density function:

$$F(\zeta) = \int_{-\infty}^{\zeta} p_\zeta(t)\mathrm{d}t. \tag{8}$$

$\Lambda(\mu)$ is related to the slope μ of the emission ray, and it is given by

$$\Lambda(\mu) = \frac{1}{\mu}\int_{\mu}^{+\infty} (\gamma - \mu) p_\gamma(\gamma)\mathrm{d}\gamma. \tag{9}$$

When deriving $S_0(\mu, \gamma_0, \zeta_0)$, the joint PDF $p(\zeta', \gamma', \zeta_0, \gamma_0)$ of the heights and the slopes of two points M' and M_0 of the surface is involved [15], where point M' is the intersection of the emission ray and the surface. Equation (7) ignores the correlation between the heights and the slopes of points M_0 and M', which means that the distributions of the slopes and the heights are independent. The joint PDF $p(\zeta', \gamma', \zeta_0, \gamma_0)$ can be expressed as the product of the corresponding PDFs:

$$p(\zeta', \gamma', \zeta_0, \gamma_0) = p_\zeta(\zeta') p_\gamma(\gamma') p_\zeta(\zeta_0) p_\gamma(\gamma_0), \tag{10}$$

where p_ζ and p_γ are the PDFs of the heights and the slopes of the surface, respectively. As a result, Eq. (7) is called the uncorrelated Smith illumination function. This correlation is considered in [16], in which the correlated Smith illumination function is also given. The mathematical expression of the correlation is not shown here because of its complexity, and the correlated illumination function is used directly in the simulations when necessary.

It is interesting to note that, for an even surface slope PDF, the shadowing term of Masuda *et al.* [1] equals mathematically the height-averaged uncorrelated illumination function of Smith. In this paper, the surface slope PDF is assumed to be Gaussian, which is even. Under such an assumption, the emissivity model of Masuda *et al.* equals the model shown here.

3. Emissivity with One Surface Reflection

A. General Expression of the Problem

The first-order emissivity (that is, with one surface reflection) corresponds to the emission energy that is reflected once on the surface before being received by the sensor. The geometry of the problem is illustrated in Fig. 2.

In Fig. 2, the point M_1 with height ζ_1 and slope γ_1 radiates an emission ray $M_1(\theta_{10})$. It reaches the surface at point M_0, and it is then reflected toward the sensor along the observation direction θ. This path is called the forward path. However, the backward path is taken in this paper to be consistent with the first-order illumination function of Li *et al.* [10]. In the backward path, an incidence ray is emitted from the sensor along the observation direction, which reaches the surface at point M_0 and is then reflected to point M_1.

The first-order emissivity corresponds to the energy emitted from point M_1, which is reflected to the observation direction by the facet at point M_0. The energy emitted at point M_0 is ignored, as it is already included in the zero-order emissivity. As a result, the first-order local emissivity of the facet at point M_0 is given by [11]

$$\varepsilon_1^{\mathrm{local}} = [1 - |r(\chi_1)_{V,H}|^2]|r(\chi_0)_{V,H}|^2. \tag{11}$$

Attention must be paid to the polarization of the first-order local emissivity. For a 1D rough surface, the emission and the reflection rays both belong to the x–z plane. The polarization state of the emission ray is not changed when it propagates to the facet of reflection. As a result, the crossed polarized terms do not contribute. In other words, the H-polarized first-order local emissivity results from the combination of $r(\chi_1)_H$ and $r(\chi_0)_H$ [HH for short, where the first H corresponds to the subscript of $r(\chi_1)$ and the second corresponds to that of $r(\chi_0)$] in Eq. (11). The same remark holds for the V-polarized first-order local emissivity. The VH and HV combinations never contribute for 1D surfaces. Thus, the first-order local emissivity is given by

$$\begin{cases} \varepsilon_{1,V}^{\mathrm{local}} = [1 - |r_V(\chi_1)|^2]|r_V(\chi_0)|^2 \\ \varepsilon_{1,H}^{\mathrm{local}} = [1 - |r_H(\chi_1)|^2]|r_H(\chi_0)|^2 \end{cases}. \tag{12}$$

The first-order emissivity is given in the same way as that of the zero-order:

$$\begin{cases} \varepsilon_{1,V} = \langle \varepsilon_{1,V}^{\mathrm{local}} g_0 S_1 \rangle_1 \\ \varepsilon_{1,H} = \langle \varepsilon_{1,H}^{\mathrm{local}} g_0 S_1 \rangle_1 \end{cases}, \tag{13}$$

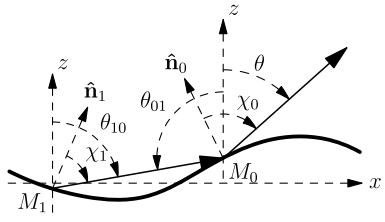

Fig. 2. Geometry of first-order emissivity (with one surface reflection).

where S_1 is the first-order illumination function, and $\langle\cdots\rangle_1$ stands for the first-order statistical average:

$$\langle\cdots\rangle_1 = \int_{-\infty}^{+\infty}\int_{-\infty}^{+\infty}\int_{-\infty}^{+\infty}\int_{-\infty}^{+\infty}\cdots \times p(\zeta_1,\gamma_1,\zeta_0,\gamma_0)\mathrm{d}\zeta_1\mathrm{d}\gamma_1\mathrm{d}\zeta_0\mathrm{d}\gamma_0, \quad (14)$$

with $p(\zeta_1,\gamma_1,\zeta_0,\gamma_0)$ being the joint PDF of the heights and the slopes of points M_1 and M_0.

In Eq. (13), the first-order local emissivity $\varepsilon_1^{\mathrm{local}}$ is derived in Subsection 3.B, while the first-order illumination function S_1 is derived in Subsection 3.C.

B. Parameters of the Geometry

In this subsection, the local incidence angle χ_1 of the surface at point M_1 is expressed in terms of the observation angle θ and of the slopes γ_0 and γ_1 of points M_0 and M_1, respectively.

With the knowledge of θ and γ_0, the unitary vector $\hat{\mathbf{m}}_{01} = (\sin\theta_{01}, \cos\theta_{01})$ of the reflection ray $M_0(\theta_{01})$ can be expressed as

$$\hat{\mathbf{m}}_{01} = 2(\hat{\mathbf{n}}_0\cdot\hat{\mathbf{m}}_0)\hat{\mathbf{n}}_0 - \hat{\mathbf{m}}_0 = 2\cos\chi_0\hat{\mathbf{n}}_0 - \hat{\mathbf{m}}_0. \quad (15)$$

Thus, the reflection angle θ_{01} is given by

$$\cos\theta_{01} = \hat{\mathbf{m}}_{01}\cdot\hat{\mathbf{z}} = 2\frac{\cos\theta-\gamma_0\sin\theta}{1+\gamma_0^2} - \cos\theta = \cos\theta[2g_0(1+\gamma_0^2)^{-1}-1]. \quad (16)$$

To obtain θ_{01}, the sign of θ_{01} must be determined. Recalling our convention that an angle is positive if measured clockwise from zenith, the sign of θ_{01}, denoted as t_1, is given by

$$\begin{cases} t_1 = +1, & \gamma_0 < -\tan(\theta/2) \\ t_1 = -1, & \gamma_0 > -\tan(\theta/2) \end{cases}.$$

The global reflection angle θ_{01} is then expressed as

$$\theta_{01} = t_1\cdot\arccos\{\cos\theta[2g_0(1+\gamma_0^2)^{-1}-1]\}, \quad (17)$$

and the slope of the reflection ray μ_1 is given by $\mu_{01} = \cot\theta_{01}$.

The global incidence angle θ_{10} of the surface at point M_1 is given by

$$\begin{cases} \theta_{10} = \theta_{01} - \pi & \text{for } \theta_{01} > 0 \\ \theta_{10} = \theta_{01} + \pi & \text{for } \theta_{01} < 0 \end{cases}. \quad (18)$$

The local incidence angle χ_1 of the surface at point M_1 is given in the same way as that for M_0:

$$\cos\chi_1 = \frac{\cos\theta_{10}-\gamma_1\sin\theta_{10}}{(1+\gamma_1^2)^{1/2}}. \quad (19)$$

With the knowledge of the local incidence angles χ_1 and χ_0 [see Eq. (2)], the first-order local emissivity can be fully evaluated. The next step is to determine the first-order illumination function.

C. First-Order Illumination Function

The key of calculating the first-order emissivity lies in determining the first-order illumination function. This paper adopts the first-order illumination function of Li *et al.* [10], as its results agree very well with the ones of a Monte Carlo ray-tracing algorithm.

The first-order illumination function gives the probability that one surface reflection occurs. It equals the probability that the emission ray $M_1(\theta_{10})$ reaches the surface at some point M_0 and the reflection ray $M_0(\theta)$ propagates toward the sensor without reaching the surface. In the model of Li *et al.* [10], the equivalent backward path is taken for convenience. It is assumed that an incidence ray is emitted from the sensor (noted M in Fig. 3), which reaches the surface at point M_0 and is then reflected to some other point M_1. With the backward path, Li *et al.* [10] defined the first-order illumination function as the probability that point M_0 is illuminated by the incidence ray [noted $P(\alpha)$], while the reflection ray reaches the surface at some point M_1 [noted $P(\beta)$]. The probability that point M_0 is illuminated by the incidence ray equals the zero-order illumination function, which means that $P(\alpha) = F(\zeta_0)^{\Lambda(\mu)}$. On the contrary, $P(\beta)$ must be determined according to four cases of single surface reflection as shown in Fig. 3.

In cases 1 and 4, the reflection ray $M_0(\theta_{01})$ propagates downward and does reach the surface, which means $P(\beta) = 1$. In cases 2 and 3, the reflection ray $M_0(\theta_{01})$ propagates upward. The probability that it reaches the surface equals the complementary probability that it does not, which means $P(\beta) = 1 - F(\zeta_0)^{\Lambda(\mu_{01})}$. To sum up, the first-order illumination function is given by [10]

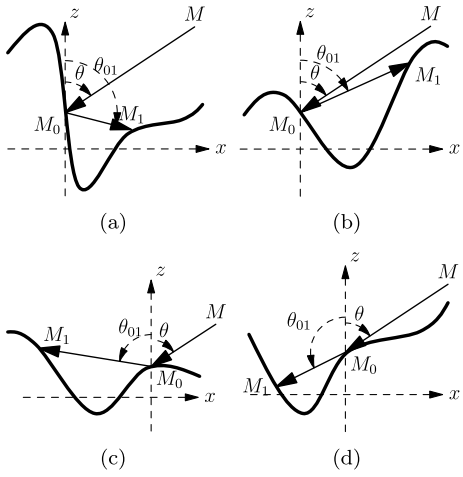

Fig. 3. Four cases of single surface reflection, with (a) case 1, the reflection ray $M_0(\theta_{01})$ propagates rightward and downward, (b) case 2, $M_0(\theta_{01})$ propagates rightward and upward, (c) case 3, $M_0(\theta_{01})$ propagates leftward and upward, and (d) case 4, $M_0(\theta_{01})$ propagates leftward and downward.

$$S_1(\mu,\zeta_0,\gamma_0)=\begin{cases} F(\zeta_0)^{\Lambda(\mu)} & 1\ \&\ 4 \\ F(\zeta_0)^{\Lambda(\mu)}[1-F(\zeta_0)^{\Lambda(\mu_{01})}] & 2\ \&\ 3 \\ 0 & \text{otherwise} \end{cases}, \tag{20}$$

where $\Lambda(\mu_{01})$ is related to the slope of the reflection ray $M_0(\theta_{01})$ and is defined by

$$\Lambda(\mu_{01})=\begin{cases} \frac{1}{\mu_{01}}\int_{\mu_{01}}^{+\infty}(\gamma-\mu_{01})p_\gamma(\gamma)\mathrm{d}\gamma, & \theta_{01}>0 \\ \frac{1}{\mu_{01}}\int_{-\infty}^{\mu_{01}}(\gamma-\mu_{01})p_\gamma(\gamma)\mathrm{d}\gamma, & \theta_{01}<0 \end{cases}. \tag{21}$$

Equation (20) neglects the correlation between the heights and the slopes of different points of the surface [10]. The determination of the correlated first-order illumination function is given in Appendix B of [10], which is not recalled here because of its complexity.

The marginal slope histogram of the first-order illumination function gives the slope distribution of point M_0. It is given by averaging $S_1(\mu,\zeta_0,\gamma_0)$ over ζ_0:

$$\bar{S}_1(\mu,\gamma_0)=\int_{-\infty}^{+\infty}S_1(\mu,\gamma_0,\zeta_0)p(\gamma_0,\zeta_0)\mathrm{d}\zeta_0. \tag{22}$$

The average first-order illumination function gives the portion of the surface for which single reflection occurs. It is obtained by averaging $S_1(\mu,\zeta_0,\gamma_0)$ over ζ_0 and γ_0:

$$\bar{\bar{S}}_1(\mu)=\int_{-\infty}^{+\infty}\int_{-\infty}^{+\infty}S_1(\mu,\gamma_0,\zeta_0)p(\gamma_0,\zeta_0)\mathrm{d}\zeta_0\mathrm{d}\gamma_0. \tag{23}$$

D. Estimation of the Slope PDF of M_1

The first-order illumination function $S_1(\mu,\zeta_0,\gamma_0)$ given in Eq. (20) is a function of the height ζ_0 and the slope γ_0 of point M_0. However, it does not depend on the height and the slope of point M_1. In fact, no information about ζ_1 or γ_1 is provided in Eq. (20), which makes it difficult to compute the statistical average in Eq. (14).

As neither the first-order local emissivity nor the first-order illumination function depends on the height of M_1, the statistical average over ζ_1 in Eq. (14) is unnecessary (the integration equals 1). However, the first-order local emissivity does depend on the slope of point M_1. As a result, the PDF of γ_1 must be determined. Li *et al.* [10] showed that to ensure $|\chi_1|<90°$, the slope γ_1 must satisfy

$$\begin{cases} \gamma_1>\mu_{01} & \text{for } \theta_{01}>0 \\ \gamma_1<\mu_{01} & \text{for } \theta_{01}<0 \end{cases}. \tag{24}$$

As no further information about γ_1 is provided, any slope checking Eq. (24) is equally considered as the slope of point M_1. The PDF of γ_1 is then given by

$$p(\gamma_1)=\begin{cases} \frac{\Upsilon(\gamma_1-\mu_{01})}{\int_{\mu_{01}}^{+\infty}p_\gamma(\gamma)\mathrm{d}\gamma}p_\gamma(\gamma_1) & \text{for } \theta_{01}>0 \\ \frac{\Upsilon(\mu_{01}-\gamma_1)}{\int_{-\infty}^{\mu_{01}}p_\gamma(\gamma)\mathrm{d}\gamma}p_\gamma(\gamma_1) & \text{for } \theta_{01}<0 \end{cases}, \tag{25}$$

where p_γ is the surface slope PDF.

With the knowledge of χ_0, χ_1, $S_1(\mu,\gamma_0,\zeta_0)$, and $p(\gamma_1)$, the first-order emissivity given in Eq. (13) can be computed.

E. Degree of Polarization

Infrared emission of a rough surface is partially polarized at large observation angles [12,13]. The DOP of the infrared emissivity is given by [12]

$$\mathrm{DOP}=\frac{\varepsilon_H-\varepsilon_V}{\varepsilon_H+\varepsilon_V}. \tag{26}$$

The magnitude of the DOP describes the fraction of the polarized component power with respect to the total power, whereas its sign relates to the dominant polarized energy. A positive DOP indicates that the globally H-polarized energy (electric vector orthogonal to x–z plane) is larger than the one globally V-polarized (electric vector in the x–z plane and orthogonal to the observation direction), and vice versa. The DOP of the sea surface infrared emissivity is computed in Section 4.

4. Numerical Results

In this section, the first-order infrared emissivity and its DOP are simulated for 1D surfaces.

It is assumed that the heights and the slopes of the surface are uncorrelated (except for the calculation of the correlated illumination function, whose mathematical expression is not shown in this paper). Under such an assumption, the knowledge of the surface height PDF is not required, as the zero- and first-order local emissivities do not depend on ζ_0 or ζ_1 [see Eqs. (3) and (13)], and averaging S_0 and S_1 over ζ_0 and ζ_1 holds for any height PDF [see Eqs. (7) and (20)].

However, the surface slope PDF is required. It is assumed that the surface slope PDF is Gaussian with zero mean:

$$p_\gamma(\gamma)=\frac{1}{\sqrt{2\pi}\sigma_\gamma}\exp\left(-\frac{\gamma^2}{2\sigma_\gamma^2}\right), \tag{27}$$

with σ_γ being the sea surface root-mean-square slope, which is estimated according to the experimental model of Cox and Munk [17]:

$$\sigma_\gamma^2\approx 3.16\times10^{-3}u_{12}, \tag{28}$$

where u_{12} is the wind speed recorded at 12.5 m above the sea level. Equation (28) only takes the upwind direction into account, as this paper considers 1D surfaces.

The infrared emissivity is simulated at wavelengths inside the infrared atmospheric windows of

3 to 5 μm and 8 to 13 μm. The sea refraction indices in these two regions are given by the model of Hale and Querry [18]: for instance, at wavelengths $\lambda = \{4; 10\}\,\mu$m, the sea refraction indices $n = \{1.3510 + 0.0046i; 1.2180 + 0.0508i\}$, respectively.

A. Evaluation of the Model

To evaluate the model, a Monte Carlo ray-tracing algorithm is used. In the ray-tracing algorithm, a 1D rough surface is generated, with Gaussian height and slope distributions. Moreover, the surface points are assumed to be correlated with a Gaussian height autocorrelation function, instead of being uncorrelated as in the model of Henderson *et al.* [9].

After the rough surface generation, an incidence ray is traced. The surface points illuminated by this incidence ray, which correspond to point M_0 in the present model, are noted, and the corresponding reflection rays at these points are traced. For the reflection rays that reach the surface again, the intersections, which correspond to point M_1, are noted. Each point M_1 and its corresponding point M_0 are called one pair. The histogram of the slope of point M_0 is calculated to obtain the slope distribution, which corresponds to the marginal slope distribution of the first-order illumination function. The Monte Carlo average first-order illumination function is given by $S_{1,\mathrm{MC}} = N_i/N_s$, where N_s is the number of points of the generated surface, and N_i is the number of pairs of points M_0 and M_1.

The Fresnel reflection coefficients at these points are calculated, and the Monte Carlo first-order emissivity is given by

$$\begin{cases} \varepsilon_{\mathrm{MC},V} = \frac{1}{N_s}\sum_{i=1}^{i=N_i}[1 - |r_V(\chi_{1,i})|^2]|r_V(\chi_{0,i})|^2 g_0 \\ \varepsilon_{\mathrm{MC},H} = \frac{1}{N_s}\sum_{i=1}^{i=N_i}[1 - |r_H(\chi_{1,i})|^2]|r_H(\chi_{0,i})|^2 g_0 \end{cases}. \quad (29)$$

Readers interested in the generation of the Gaussian rough surface and the construction of the ray-tracing algorithm can refer to [16,11].

It is recalled that the zero- and first-order illumination functions given in Eqs. (7) and (20) neglect the correlation between the heights and the slopes of distinct surface points [10,15]. The agreements between the analytical models and the reference are improved by taking the correlation into account [10,16]. To study the correlation effect, the first-order infrared emissivity with the correlated first-order illumination function is also simulated in this paper, without showing its complex mathematical expression (see [10]).

B. First-Order Illumination Function

The first-order illumination function of Li *et al.* [10], for uncorrelated [Eq. (20)] and correlated {Eqs. (16), (B6) of [10]} height and slope PDFs, is used in this subsection. The results are compared with the ones obtained by the Monte Carlo ray-tracing algorithm.

The simulation is performed for wind speeds $u_{12} = \{5; 10\}$ m/s. The marginal slope histogram of the first-order illumination function [Eq. (22)] is simulated and shown in Fig. 4(a), for an observation angle of 80°. The average first-order illumination function (23) is shown in Fig. 4(b).

It can be observed in Fig. 4(a) that the slope distribution of M_0 given by the model of Li *et al.* agrees well with the Monte Carlo result, even if an uncorrelated slope PDF is considered. Consequently, the portion of the surface for which single surface reflections occur as predicted by the model agrees well with the result of the Monte Carlo algorithm [see Fig. 4(b)]. It is shown that surface reflections occur at large observation angles, for example, at $\theta > 50°$ for $u_{12} = 5$ m/s.

It is noticeable that the uncorrelated model slightly overestimates the surface reflection effect. However, very good agreement is observed when a correlated height and slope PDF is considered.

C. First-Order Infrared Emissivity

The first-order infrared emissivity is calculated according to Eq. (14), where the local incidence angles χ_0 and χ_1 are given by Eqs. (2) and (19), respectively. The first-order illumination function is given by Eq. (20). The results are shown in Fig. 5.

It is shown that the first-order infrared emissivity contributes at large observation angles. Employing

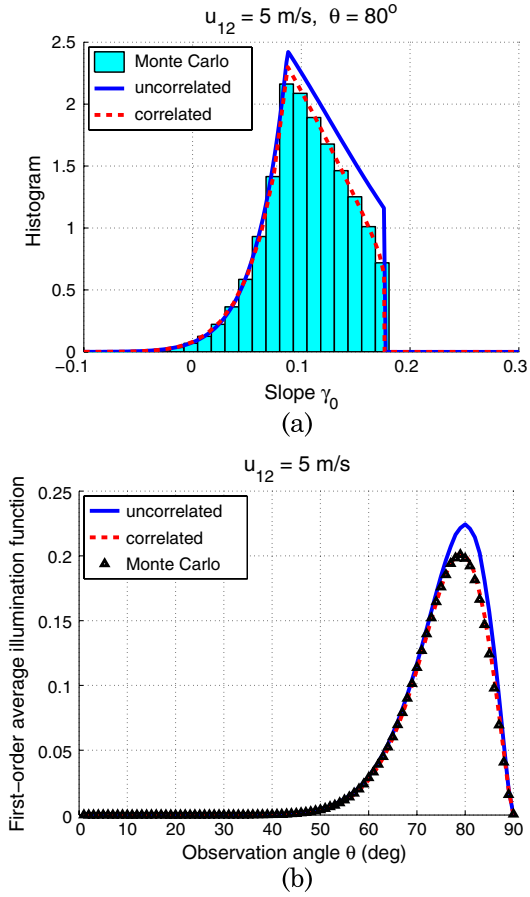

Fig. 4. (Color online) Marginal slope histogram of the (a) first-order illumination function and (b) average first-order illumination function.

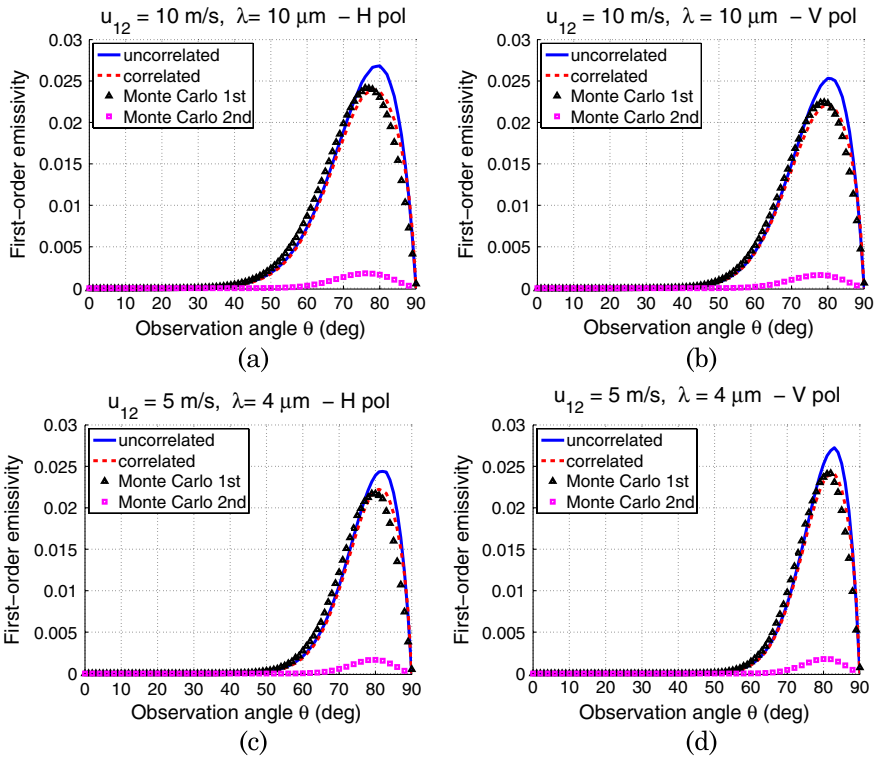

Fig. 5. (Color online) First-order emissivity for $u_{12} = 10\,\mathrm{m/s}$, $\lambda = 10\,\mu\mathrm{m}$ [(a) H polarization, (b) V polarization], and $u_{12} = 5\,\mathrm{m/s}$, $\lambda = 4\,\mu\mathrm{m}$ [(c) H polarization, (d) V polarization].

the uncorrelated first-order illumination function, the present model predicts the first-order emissivity quite well for both H and V polarizations. The first-order emissivities for H and V polarizations are slightly overestimated at large observation angles. This was predictable, as the adopted uncorrelated first-order illumination function slightly overestimates the surface reflection effect at these angles [see Fig. 4(b)].

The agreements are significantly improved when the correlated first-order illumination function is employed. However, the agreements are not as good as that shown in Fig. 4(b), unexpectedly. For both H and V polarizations, the present model using the correlated first-order illumination function slightly overestimates the first-order emissivity at large observation angles ($\theta > 80°$ in Fig. 5), while underestimating it at smaller observation angles ($\theta < 80°$ in Fig. 5).

A closer look at Eq. (13) helps us explain this deviation. Indeed, the first-order emissivity depends on three terms: the first-order local emissivity, the area projection term g_0, and the first-order illumination function. It has already been observed in Subsection 4.B that the first-order illumination function works very well and that the slope distribution of point M_0 is also well predicted. As g_0 depends only on the slope of point M_0 and on the observation angle θ, it should not be the source of the error. As a result, the discrepancy should come from the first-order local emissivity, which depends on the slopes of points M_0 and M_1. As the distribution of γ_0 is well predicted by the first-order illumination function [see Fig. 4(a)], the error mainly comes from the fact that the definition of the PDF of γ_1 is not precise.

The PDF of γ_1 is given in Eq. (25), which is based on the assumption that all the slopes which fulfill the prerequisite "the local incidence angle χ_1 is not larger than 90° in absolute value" could equally be the slope of point M_1. Until now, no rigorous proof is found to support this assumption. However, as little knowledge about γ_1 is given by the first-order illumination function, this problem is left to future work.

Referring to the Monte Carlo ray-tracing method, the first-order emissivity has a maximum of about 2.5×10^{-2} and tends to zero at $\theta = 90°$. However, the first-order emissivity of Masuda (Fig. 3 of [8], noted $r_1^\star$) reaches a maximum of about 5×10^{-2}, which is nearly twice the maximum of the Monte Carlo result. In addition, it does not equal zero at $\theta = 90°$, while the Monte Carlo result does. There are two possible reasons for the appearance of this discrepancy. First, Masuda used a weighting function to estimate the probability of observing one surface reflection, which is built on a shadowing term. The shadowing term gives the proportion that the surface is illuminated, which does not equal the probability that a certain point is illuminated and which is not suitable for extension to higher orders. The second reason is that Masuda used the direct emissivity of the surface at $\theta > 90°$. In this region, the sensor is below the sea surface, which is not physical.

The Monte Carlo ray-tracing method for calculating the second-order infrared emissivity (with two surface reflections) is also developed, and the corresponding results are shown in Fig. 5 (squares). A maximum of about 2.5×10^{-3} at 80° is observed for both H and V polarizations, which is less than the sensitivity requirement 5×10^{-3} reported by Wu and Smith [4]. The Monte Carlo results for calculating three surface reflections are also computed, which show a maximum of about 4×10^{-4} (not plotted here). As a result, the second and higher order infrared emissivities are negligible for our application.

D. Total Emissivity of the Surface

The total infrared emissivity is obtained by summing up the zero- and first-order ones, whereas the higher orders are ignored. Although the first-order emissivity model using the correlated first-order illumination function better agrees with the Monte Carlo result than that using the uncorrelated one, the uncorrelated model is considered because of its significantly lower time consumption. Figure 6 shows the uncorrelated zero-order and total emissivities of the surface for wind speed $u_{12} = 10\,\mathrm{m/s}$ and wavelength $\lambda = 10\,\mu\mathrm{m}$. The results for $u_{12} = 5\,\mathrm{m/s}$ and for $\lambda = 4\,\mu\mathrm{m}$ are not shown as they lead to the same observations and conclusions.

It is shown that the total emissivity of the sea surface decreases with the observation angle. Compared with the zero-order emissivity, the total emissivity is significantly increased at large observation angles by taking the first-order emissivity into account. The analytical results agree well with the Monte Carlo results, except for gazing angles ($\theta > 80°$).

E. Degree of Polarization

To study the polarization state of the sea surface emissivity, the DOP of the zero-order, first-order, and total infrared emissivities are calculated according to Eq. (26) and plotted in Fig. 7. The results for $u_{12} = 5\,\mathrm{m/s}$ and for $\lambda = 4\,\mu\mathrm{m}$ are not shown, as they lead to the same conclusions.

Figure 7(a) shows the DOP of the first-order infrared emissivity of the sea surface. It is shown that the first-order infrared emissivity ε_1 can be highly polarized at small to moderate observation angles [up to 65% at $\theta \approx 40°$ in Fig. 7(a)], although the magnitude

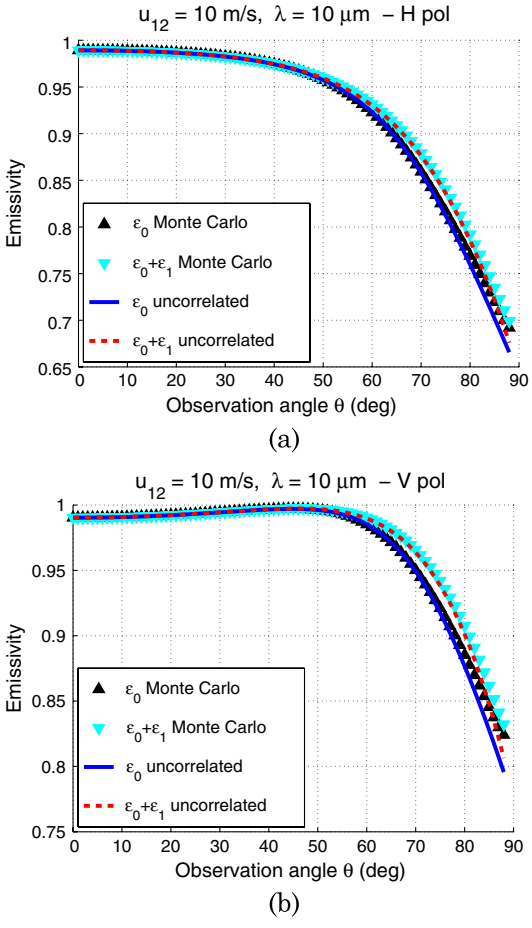

Fig. 6. (Color online) Uncorrelated zero-order emissivity of the surface (solid curve) and the corresponding Monte Carlo result (triangles), and the total emissivity of the surface (dashed curve) and the corresponding Monte Carlo result (wedges) for (a) H polarization and (b) V polarization.

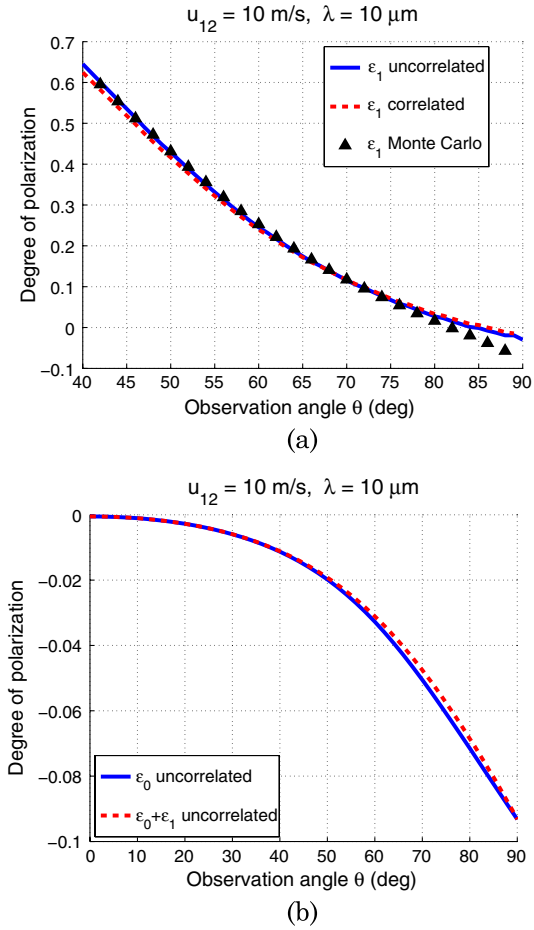

Fig. 7. (Color online) (a) DOP of the first-order infrared emissivity of the sea surface and the comparison between the DOPs without surface reflections [zero-order, solid curve in (b)] and with one surface reflection [total, dashed curve in (b)].

of ε_1 is close to zero and very small compared to ε_0 (see Figs. 5 and 6). The DOP of ε_1 decreases to zero at $\theta \approx 85°$, and continuously decreases to about -5% at $\theta = 90°$. In other words, for the polarized component of the first-order infrared emissivity, the globally H-polarized energy is the majority for $\theta < 85°$, while the globally V-polarized energy is the majority for $\theta > 85°$. At $\theta \approx 85°$, the first-order infrared emissivity is unpolarized.

Figure 7(b) shows the DOPs of the uncorrelated zero-order and total infrared emissivities of the sea surface. It is shown that the DOP of the total infrared emissivity of the surface is negative and decreases to about -9% as the observation angle increases to $\theta = 90°$, which means that the globally V-polarized energy is the majority, and that up to 9% of the energy is polarized at $\theta = 90°$. The DOP of the total surface emissivity is slightly reduced in magnitude at large observation angles, which means that surface reflections (slightly) reduce the polarization feature of the surface radiation.

F. Comparison with Measurements of Smith *et al.*

Smith *et al.* [5] derived the sea surface infrared emissivity from measurement data in the Gulf of Mexico at 16 January 1995. The results were compared in [5] with those of the zero-order emissivity model of Masuda *et al.* [1] at three observation angles $\theta = \{36.5°, 56.5°, 73.5°\}$. It was reported in [5] that the zero-order infrared emissivity model underestimates the infrared emissivity of about 3×10^{-2} at 73.5°, and of about 5×10^{-3} at 56.5°. Differences are not significant at 36.5°. In this section, the first-order infrared emissivity is taken into account in order to improve the agreement between analytical models and measurement data.

It is recalled that the Smith illumination function is used here to derive the zero-order emissivity, whereas Smith *et al.* compared their data with those obtained by the model of Masuda *et al.* [5]. However, no difference is introduced, as these two methods equal each other under the assumption that the surface slope PDF is Gaussian.

The experiment of Smith *et al.* was conducted under a wind speed ranging from 2 to 8 m/s (see [5], Fig. 9, the region for 16 January 1995). To make a comparison, the wind speed is set to the average wind speed of the experiment $u_{12} = 5$ m/s in our simulation. Unpolarized emissivity is compared. In the simulation, the sea surface unpolarized emissivity is obtained by averaging the ones in H and V polarizations. The sea refraction indices are given by the model of Hale and Querry [18]. The result is shown in Fig. 8, for wavenumbers 850–1150 cm^{-1}, which corresponds to wavelengths 8.7–11.8 μm.

It is observed that the agreement is greatly improved by taking the first-order emissivity into account at the observation angle $\theta = 73.5°$. The maximum error is observed at about $k \approx 900\ \text{cm}^{-1}$ ($\lambda = 11\ \mu$m). A small improvement is also observed at $\theta = 56.5°$. Taking the first-order emissivity into account at $\theta = 36.5°$ does not make any difference, as it is negligible at small observation angles (see Fig. 5).

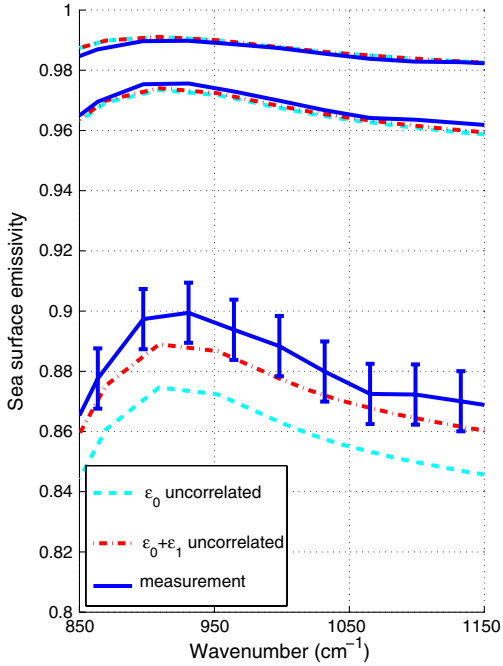

Fig. 8. (Color online) Comparison with measurements by Smith *et al.* [5] at observation angles of 36.5° (upper), 56.5° (intermediate), and 73.5° (lower). The measurement data are taken from Fig. 10 of [5]. Simulation is made under a wind speed of 5 m/s.

G. Comparison with Measurements of Niclòs *et al.*

Niclòs *et al.* [6] derived the infrared emissivity of the open Mediterranean sea surface from an oil rig. Radiometric data were taken by a CE 312 radiometer with four wavelength channels: 8–14, 8.2–9.2, 10.5–11.5, and 11.5–12.5 μm. Sea surface emissivity was determined for observation angles ranging from 25° to 65°, with a step of 10°. The wind speeds over the sea surface were approximately $u_{12} = \{4.5 \pm 0.9; 10.3 \pm 1.1\}$ m/s.

To make a comparison, the unpolarized sea surface infrared emissivity is simulated under similar conditions for the three channels of wavelength: 8.2–9.2, 10.5–11.5, and 11.5–12.5 μm. For channel 8.2–9.2 μm, the emissivities are obtained for wavelengths with a step of 0.2 μm, whereas for channels 10.5–11.5 and 11.5–12.5 μm, a step of 0.5 μm is taken. The emissivity of each channel is computed by averaging the ones of wavelengths within it. The wind speed in the simulation is set to $u_{12} = \{4.5, 10.3\}$ m/s. The results are shown in Fig. 9.

It can be observed that the zero-order emissivity agrees well with the measurements at small observation angles $\theta \leq 55°$. An underestimation is observed at $\theta = 65°$. The agreement is improved by taking the first-order emissivity into account, except for the case shown in Fig. 9(d).

The measurements of Smith *et al.* [5] and Niclòs *et al.* [6] correspond to a real two-dimensional (2D)

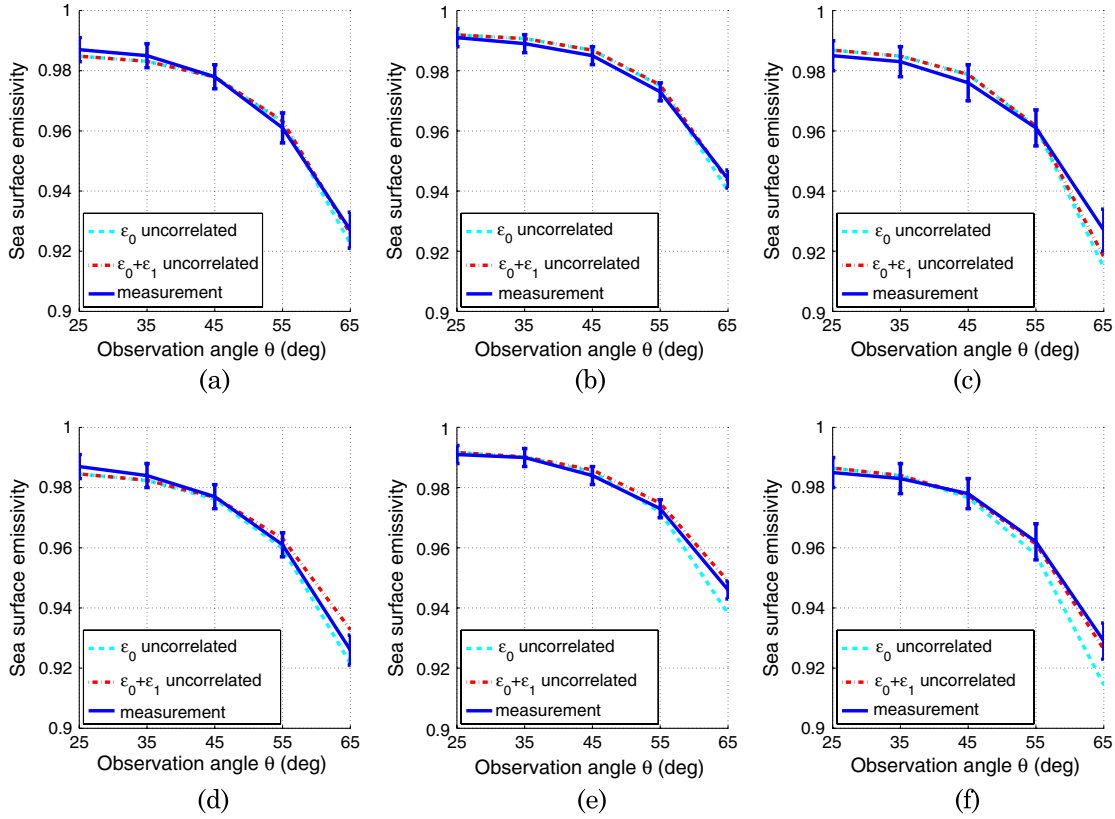

Fig. 9. (Color online) Comparison with measurements by Niclòs *et al.* at wind speeds of 4.5 m/s [(a)–(c)] and 10.3 m/s [(d)–(f)]. Three wavelength channels are considered: 8.2–9.2 μm [(a) and (d)], 10.5–11.5 μm [(b) and (e)], 11.5–12.5 μm [(c) and (f)].

sea surface, whereas the present model considers 1D surfaces. However, it turns out that the results of the 1D model agree well with the measurements of a 2D surface. Meanwhile, a 1D model is simpler than a 2D model in its mathematical expression and easier to simulate. As a result, the 1D model is more attractive.

5. Conclusion

Surface reflection is an important phenomenon when estimating the sea surface infrared emissivity, and in particular at large observation angles. This paper calculates the first-order (that is, with one surface reflection) infrared emissivity, which is compared with a Monte Carlo ray-tracing method. It is shown that the present model agrees well with the Monte Carlo result, especially when the correlation between the surface heights and slopes is considered. In addition, the agreement between the analytical model and measurements is greatly improved by taking one surface reflection into account, especially at large observation angles. It is also shown that the emissivity with two and three reflections is of the order of 2.5×10^{-3} and 4×10^{-4}, respectively, which is negligible. Polarization is also studied. It is shown that the first-order and the total sea surface emissivities are partially polarized. Studying the polarized part, the globally H-polarized first-order emission energy is the majority at small observation angles, while the globally V-polarized one is the majority at large observation angles. However, for the total emission of the sea surface, the globally V-polarized component is always the majority. One surface reflection (slightly) reduces the polarization feature of the total infrared emissivity of the surface.

References

1. K. Masuda, T. Takashima, and Y. Takayama, "Emissivity of pure and sea waters for the model sea surface in the infrared window regions," Remote Sens. Environ. **24**, 313–329 (1988).
2. C. Bourlier, "Unpolarized infrared emissivity with shadow from anisotropic rough sea surfaces with non-Gaussian statistics," Appl. Opt. **44**, 4335–4349 (2005).
3. S. Fauqueux, K. Caillault, P. Simoneau, and L. Labarre, "Multiresolution infrared optical properties for Gaussian sea surfaces: Theoretical validation in the one-dimensional case," Appl. Opt. **48**, 5337–5347 (2009).
4. X. Wu and W. L. Smith, "Emissivity of rough sea surface for 8–13 μm: Modeling and verification," Appl. Opt. **36**, 2609–2619 (1997).
5. W. L. Smith, R. O. Knuteson, H. E. Revercomb, W. Feltz, N. R. Nalli, H. B. Howell, W. P. Menzel, O. Brown, J. Brown, P. Minnett, and W. McKeown, "Observations of the infrared radiative properties of the ocean implications for the measurement of sea surface temperature via satellite remote sensing," Bull. Am. Meteorol. Soc. **77**, 41–51 (1996).
6. R. Niclòs, E. Valor, V. Caselles, C. Coll, and J. M. Sanchez, "*In situ* angular measurements of thermal infrared sea surface emissivity—validation of models," Remote Sens. Environ. **94**, 83–93 (2005).
7. P. D. Watts, M. R. Allen, and T. J. Nightingale, "Wind speed effects on sea surface emission and reflection for the along

track scanning radiometer," J. Atmos. Ocean. Technol. **13**, 126–141 (1996).
8. K. Masuda, "Infrared sea surface emissivity including multiple reflection effect for isotropic Gaussian slope distribution model," Remote Sens. Environ. **103**, 488–496 (2006).
9. B. G. Henderson, J. Theiler, and P. Villeneuve, "The polarized emissivity of a wind-roughened sea surface: A Monte Carlo model," Remote Sens. Environ. **88**, 453–467 (2003).
10. H. Li, N. Pinel, and C. Bourlier, "A monostatic illumination function with surface reflections from one-dimensional rough surfaces," Waves Random Complex Media **21**, 105–134 (2011).
11. C. Bourlier, "Unpolarized emissivity with shadow and multiple reflections from random rough surfaces with the geometric optics approximation: Application to Gaussian sea surfaces in the infrared band," Appl. Opt. **45**, 6241–6254 (2006).
12. J. A. Shaw, "Degree of linear polarization in spectral radiances from water-viewing infrared radiometers," Appl. Opt. **38**, 3157–3165 (1999).
13. J. Shaw and C. Marston, "Polarized infrared emissivity for a rough water surface," Opt. Express **7**, 375–380 (2000).
14. N. Pinel and C. Bourlier, "Scattering from very rough layers under the geometric optics approximation: further investigation," J. Opt. Soc. Am. A **25**, 1293–1306 (2008).
15. B. Smith, "Geometrical shadowing of a random rough surface," IEEE Trans. Antennas Propag. **15**, 668–671 (1967).
16. C. Bourlier, G. Berginc, and J. Saillard, "Monostatic and bistatic statistical shadowing functions from a one-dimensional stationary randomly rough surface according to the observation length: I. single scattering," Waves Random Complex Media **12**, 145–173 (2002).
17. C. Cox and W. Munk, "Measurement of the roughness of the sea surface from photographs of the sun's glitter," J. Opt. Soc. Am. **44**, 838–850 (1954).
18. G. M. Hale and M. R. Querry, "Optical constants of water in the 200 nm to 200 μm wavelength region," Appl. Opt. **12**, 555–563 (1973).